Cambridge Centre for Computational Chemical Engineering

University of Cambridge

Department of Chemical Engineering

Preprint ISSN 1473 – 4273

Numerical Simulations of Soot Aggregation in Premixed Laminar Flames

Neal Morgan[1], Markus Kraft[1], Michael Balthasar[2], David Wong[3],

Michael Frenklach[3] Pablo Mitchell[3]

submitted: May 2, 2006

[1] Department of Chemical Engineering
University of Cambridge
Cambridge CB2 3RA,
UK
E-mail: mk306@cam.ac.uk

[2] Volvo Technology Corporation
Dept. 6180, CTP,
Sven Hulins Gata 9A,
SE-412 88 Gothenburg,
Sweden

[3] Department of Mechanical Engineering, University of California,
Berkeley, CA 94720-1740, USA, and
Environmental Energy Technologies Division, Lawrence Berkeley National Laboratory,
Berkeley, CA 94720, USA

Preprint No. 37

c4e

Key words and phrases. Soot, Laminar Premixed Flames, Structural Evolution, Stochastic Modelling.

Edited by
Cambridge Centre for Computational Chemical Engineering
Department of Chemical Engineering
University of Cambridge
Cambridge CB2 3RA
United Kingdom.

Fax: + 44 (0)1223 334796
E-Mail: c4e@cheng.cam.ac.uk
World Wide Web: http://www.cheng.cam.ac.uk/c4e/

Abstract

In this paper we make use of a detailed particle model and stochastic numerical methods to simulate the particle size distributions of soot particles formed in laminar premixed flames. The model is able to capture evolution of mass and surface area along with the full structural detail of the particles. The model is validated against previous models for consistency and then used to simulate flames with bimodal and unimodal soot particle distributions. The change in morphology between the particles from these two types of flames provides further evidence of the interlay among nucleation, coagulation, and surface rates. The results confirm the previously proposed role of the strength of the particle nucleation source in defining the instant of transition from coalescent to fractal growth of soot particles.

Contents

1 Introduction

It has long been known that the size and shape of nanoparticles directly affect their physical properties. The mechanism for their growth has been investigated under many conditions and for a variety of chemical systems [18, 26, 27, 8, 13, 6, 3]. In most cases there is an initial phase of coalescent growth [11], where coagulation with small particles caused by high particle inception and rapid surface growth cause the particles to grow into near spherical "primary" particles. The coalescent regime is followed by particle aggregation, when the particles take on the form of fractal aggregates [15, 14, 20].

Many numerical techniques have been developed for the simulation of populations of nanoparticles [16] and, in particular, soot particles. Here we focus on stochastic particle methods. In recent applications of this general approach, particle dynamics were formulated in terms of one or two state variables like total particle volume and surface area [3, 10, 25, 24]. In another development, a collector-particle technique was applied to investigate the transition between coalescent and aggregate growth [22, 23], with the results incorporated [2] into the method of moments [6].

In the present study we combine two techniques, the efficient stochastic particle collision algorithm [3, 10] and the sterically-resolved collector-particle simulations [22, 23]. In the following, we describe the numerical model, test the accuracy and authenticity of model predictions, and then perform a series of numerical simulations of time evolution of soot particles and their size distribution.

2 Model

The population balance is governed by three main elements: particle nucleation, coagulation, and surface growth. In the present model, each incepted particle is defined as a sphere with center of mass in cartesian coordinates $(x = 0, y = 0, z = 0)$, a radius r_0, volume v_0 and surface area a_0. When an event affects this particle, one or more of its internal coordinates will change. A surface event for example will change v, a and r, whilst a coagulation event will displace the (x, y, z) coordinates of one of the coagulating pair.

The rate of particle nucleation in the model is determined by the rate of binary collisions of gaseous pyrene molecules [31, 7]. A detailed gas phase chemistry model that describes the formation of pyrene is taken from Refs. [30, 1].

The coagulation is governed by the Smoluchowski coagulation equation [29] with a suitable kernel, as described in the next section, to calculate the rates of collisions of the particles at the temperatures and pressures investigated.

The surface processes include chemical growth and oxidation as well as physisorption of pyrene [9, 7]. The chemical growth is modelled as the addition of acetylene to a radical site on the particle's surface through the hydrogen abstraction carbon

addition (HACA) mechanism [7]. The condensation of pyrene onto the surface of a soot particle is modelled as a coagulation event between a pyrene molecule and the particle of interest [9, 31, 19]. Oxidation of a particle is considered as the reaction of O_2 with surface radicals or the reaction of OH with the surface of the particle [9, 7]. The surface growth kinetics are taken from [1].

3 Numerical treatment

The model defined above is solved using a stochastic particle algorithm [3, 10]. The efficiency of the algorithm has been vastly improved by use of a time-splitting technique for the fast surface growth processes, and by introducing a majorant kernel [10, 5] for the coagulation term. Another important feature of the new code is the ability to handle essentially an infinite number of internal coordinates, thereby tracking the positions and radii of every primary particle of the aggregate structure. This, in turn, allows us to determine the particle volume, surface area, collision diameter, and fractal dimension distributions throughout the flame.

There are two input files required for the simulation. The first, supplies species concentrations and flame temperature as functions of reaction time, while the second file specifies details of the simulation, such as the final time and the time for splitting the processes.

The time between events, τ, is generated as an exponential distribution with parameter equal to the sum of inception rate and the total coagulation rate. The calculation of the total coagulation rate requires a summation over all possible collision pairs. This summation normally takes of the order N^2 operations, where N is the number of stochastic particles, because of the mathematical form of the coagulation kernel, $K(x, y)$, where x and y are representative particle properties. However, if the coagulation kernel can be represented as the product of two independent terms, we can reduce this complexity to the order of N. Such a majorant kernel, $\hat{K}(x, y)$, must satisfy the inequality

$$\hat{K}(x, y) \geqslant K(x, y) \quad \forall\, x, y. \tag{3.1}$$

This results, however, in an over-prediction of the coagulation rate. To correct for this, we introduce "fictitious jumps", when time advances, but no coagulation event is performed. A fictitious jump is performed with probability $K/\hat{K}$. For further details on the form of the majorant kernel see Ref. [10].

A coagulation event, is performed by summing the volumes and surface areas of the two aggregates picked. This is accomplished with the code of Mitchell [21], which performs a ballistic collision in $\mathbb{R}^3$ and, based on the point of contact of the newly formed pair, translates the coordinates of the primary particles of one of the aggregates relative to the other particle.

Particle nucleation, adds a spherical particle of size 32 carbon atoms.

Surface growth, is performed over an interval dt which is typically a value of $1/100^{\text{th}}$

to $1/1000^{\text{th}}$ of the final simulation time. The rates of the surface processes are calculated for each particle using the gas-surface rates [1] and the surface areas of the particles. From these rates a mean number of events for each particle for interval dt is calculated. This number is then used as a parameter for a poisson random process to determine the actual number of events that should have occurred (for more details on this see [24]). The corresponding number of carbon atoms is added to the aggregate and by considering the density of soot and the surface area of the aggregate, each primary particle is also increased in radius. The surface area of the particle, its radius of gyration, and fractal dimension are then recalculated with Monte-Carlo integration routines over the whole aggregate [21]. If through oxidation the number of carbon atoms in an aggregate falls to below 32 then this particle is considered "oxidized" and is removed from the system [6, 3].

4 Validation

The numerical implementation of the model was compared to a previously validated one-dimensional (1-D) stochastic code in order to verify that the surface growth routines had been implemented correctly. Both simulations were run using 2^{18} stochastic particles, with particle inception, coagulation, and surface growth included. The new routines produced results in very close agreement to the previous code, the error in the first moment arising from the numerical splitting routine being only 1%.

The code was also run in pure coagulation mode to verify that the fractal dimensions calculated are in agreement with previous values in the literature. Figure 1 shows the results of this simulation. The x-axis shows the ratio of collision diameter, D_c, to the primary particle diameter, D_p, while the y-axis shows the number of primary particles, n_p. In this paper, D_c is defined to be twice the radius of gyration of the particle. The circles on the diagram represent individual particles in the simulation. The primary particle diameter is calculated from [28]

$$D_\mathrm{p} = 6v/a, \tag{4.1}$$

while the number of primaries can be determined by dividing the volume by the volume of a primary

$$n_\mathrm{p} = \frac{6v}{\pi D_\mathrm{p}^3} = \frac{a^3}{36\pi v^2}, \tag{4.2}$$

where v and a are the volume and surface area of the aggregate particle, respectively. The calculated fractal dimension for this simulation was 1.93, in accordance with the result from the simulations in Ref. [12], which reported a value of 1.91 ± 0.03 using a similar ballistic cluster-cluster aggregation model.

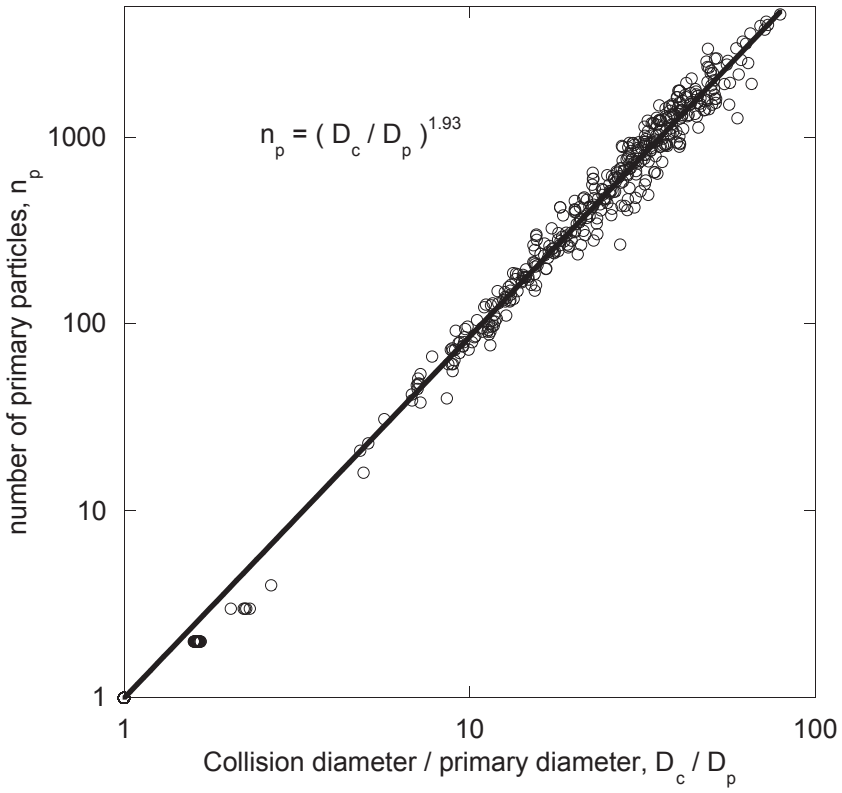

Figure 1: A plot of $D_{\rm c}/D_{\rm p}$ vs $n_{\rm p}$ for a pure coagulation simulation.

5 Results

Two sooting laminar premixed flames were simulated. The flame properties were taken from Zhao et al. [32] and are summarized in Table 1. These flames were chosen for their short residence times and because they included both unimodal and bimodal particle size distributions.

Table 1: Summary of flame conditions [32].

Flame code	Mol% gases $C_2H_4/O_2/Ar$	cold gas vel. (cm/s)	Tmax (K)
A1	24.2/37.9/37.9	7.0	1790
A3	24.2/37.9/37.9	10.0	1920

A simulation was performed to compare the full three-dimensional (3-D) particle aggregation model with the simpler, particle coalescence-only model. A comparison of the number density and soot volume fraction of the particle distribution is shown in Fig. 2. As expected, at the early stages of the flame, when the particles are in

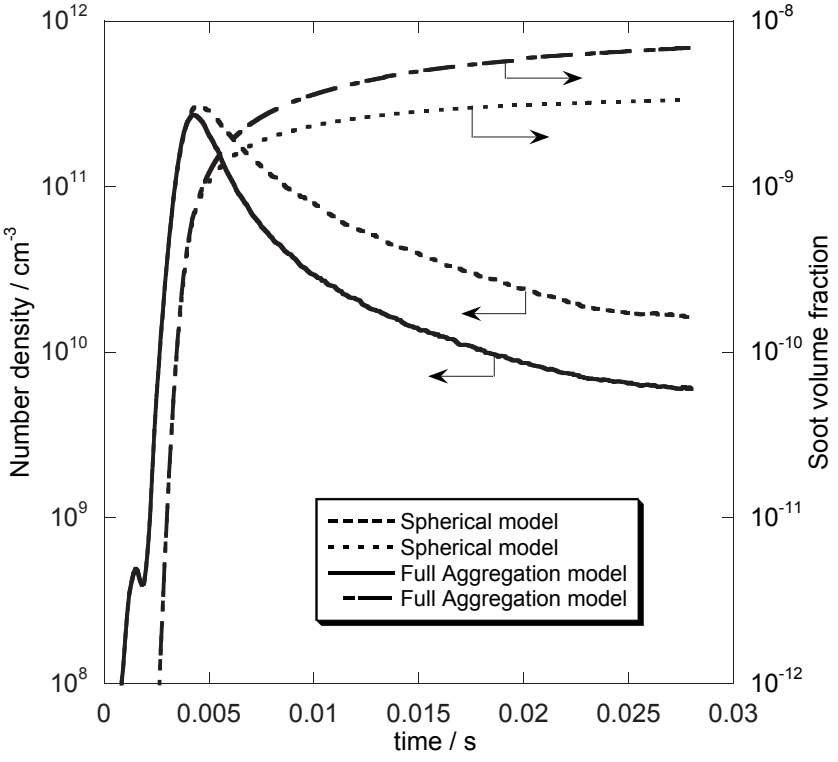

Figure 2: Comparison of number density and volume fraction between the aggregation model and the coalescent-sphere model.

the coalescent growth regime, the two simulations agree closely. After 4 ms the aggregation phase of growth begins and the number of particles falls more rapidly

in the particle aggregation simulation than in the coalescence-only simulation. This is entirely due to the fact that the collision diameters of the particles are greater in the aggregation simulations and hence the rate of coagulation is greater. It can be seen also that the total volume of particles in the system is increased when using the aggregation simulations. This is due to the fractal aggregate particles having greater surface area than the equivalent spherical particles, hence the surface growth processes occur at a much greater rate. These features are similar to previous modelling studies [13, 2].

Figure 3 shows the particle size distribution functions (PSDFs) of the volume equivalent sphere diameter, D_{v}, for flames A1 and A3 at 28 and 18 ms respectively (solid lines) plotted against the corresponding experimental data of Zhao et al. [32](circles). We can see in Fig. 3(a) that flame A1 exhibits a bimodal PSDF whilst Fig. 3(b) shows that flame A3 exhibits a unimodal distribution. This behavior is captured by the model however it predicts a broader PSDF. This is due in part to the original model being optimized for a spherical particle description, rather than one where the full morphology of the particles is calculated. This leads to an overprediction of the coagulation and surface growth rates.

Figure 4 shows how various mean particle properties evolve throughout the flames. It is observed that the average collision diameter and the average primary particle diameter are smaller in flame A1 than in flame A3, furthermore the calculated number of primary particles is higher in flame A1 than A3. It can be seen in Fig. 5 that the aggregate from flame A1 (Fig. 5(a)) appears to have larger primary particles than the aggregate from flame A3 (Fig. 5(b)). However, the primary particles from the aggregate of flame A1 are considerably "bumpier" and hence have greater surface area than those of flame A3. Since the primary particle diameter was calculated using Eq. (4.1) it is clear that the calculated primary diameter will be smaller. This indicates one of the disadvantages of using Eq. (4.1) to calculate a primary particle diameter with particles of a morphology observed in Fig. 5(a).

Figures 7 and 8 show renderings of the largest particles obtained in the simulations of flames A1 and A3. The TEM-style rendering is of the same particle shown in the 3D rendering, but from a different angle. Note that the primary particle size for both particles is unchanged from the renderings seen in Fig. 5.

Figure 6 shows the temporal evolution of the average fractal dimension, D_{f}, and the average shape descriptor, D_{s}, defined by

$$D_s = \frac{\log(a/a_0)}{\log(v/v_0)}. \tag{5.1}$$

It can be seen that the average shape descriptor starts at a value of $0.66\dot{6}$, quickly rises, and then slowly asymptotes to a value of about 0.735. This value is approximately the same for both flames. The average fractal dimension for both flames starts from a value of 3, which then falls off rapidly and eventually asymptotes to a final value. In the case of flame A1, the final value is $D_{\mathrm{f}} = 2.348$, while for flame A3 the final value is $D_{\mathrm{f}} = 2.160$. This is consistent with the observations of Fig. 5,

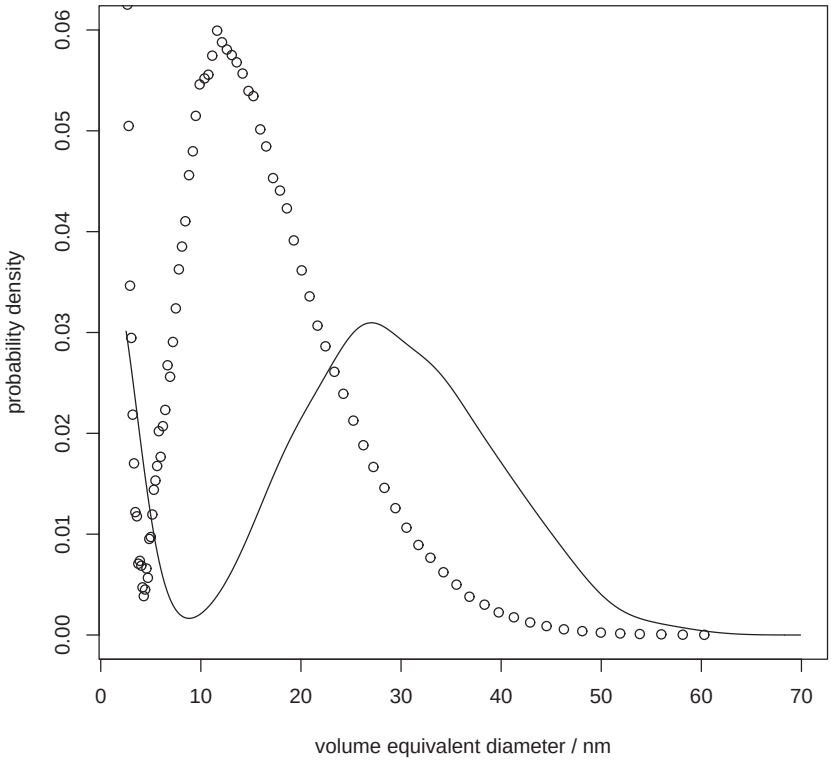

(a) *PSDF of D_v for flame A1*

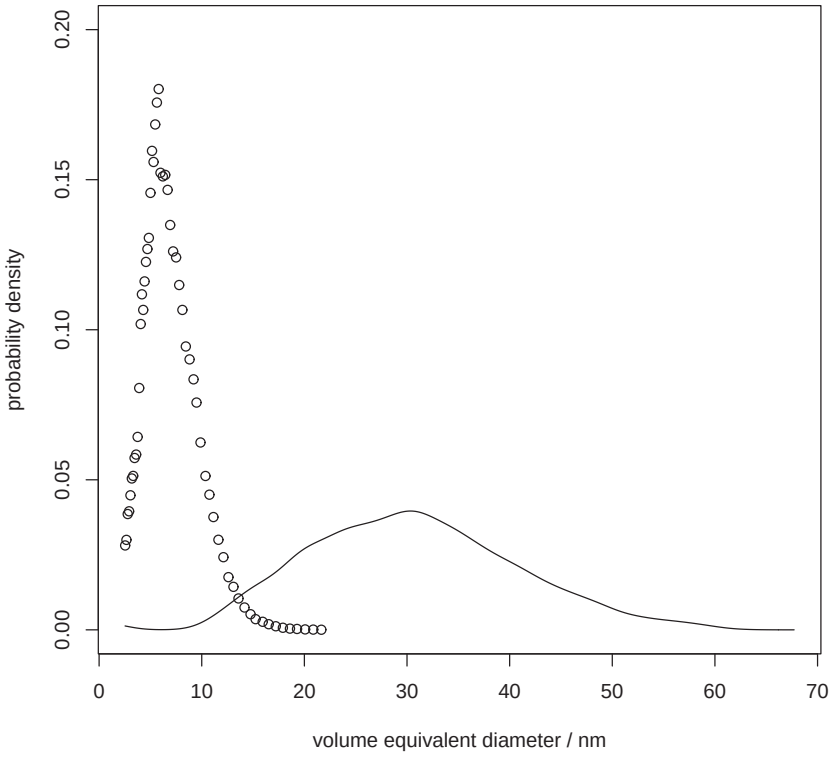

(b) *PSDF of D_v for flame A3*

Figure 3: *PSDFs of D_v from flames A1 and A3: Simulations (solid lines) and experiments (circles).*

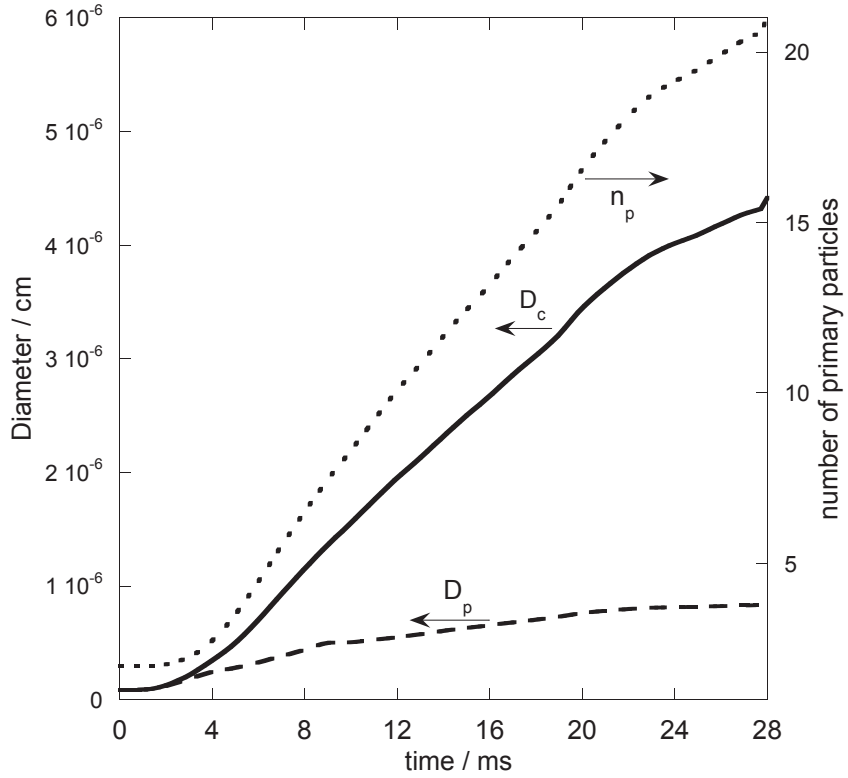

(a) *Temporal evolutions of average D_{c}, D_{p} and n_{p} in flame A1*

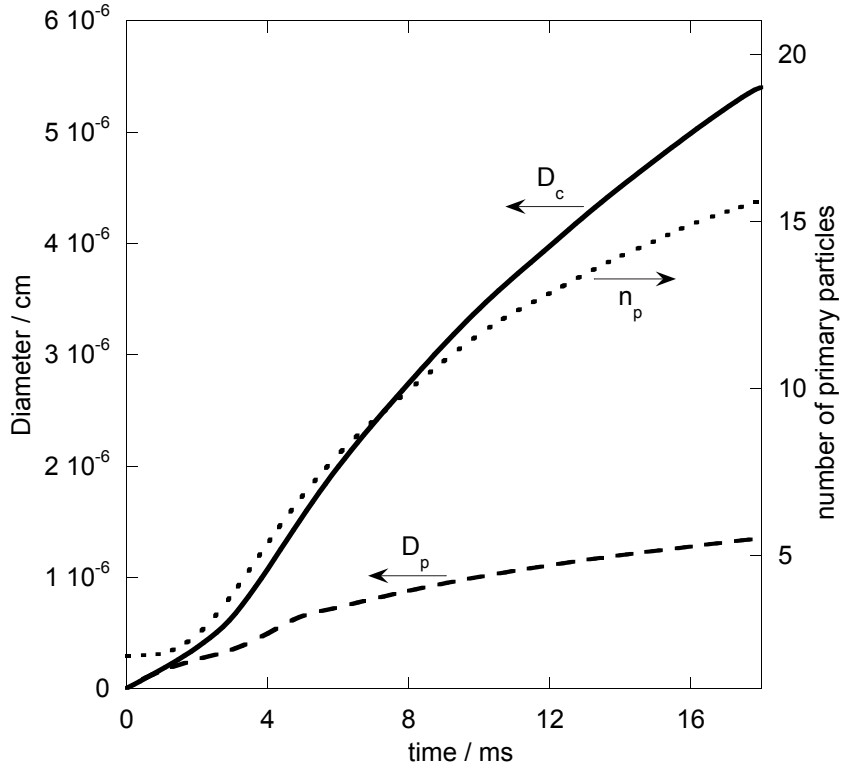

(b) *Temporal evolutions of average D_{c}, D_{p} and n_{p} in flame A3*

Figure 4: *Temporal evolution of particle properties for flames A1 and A3.*

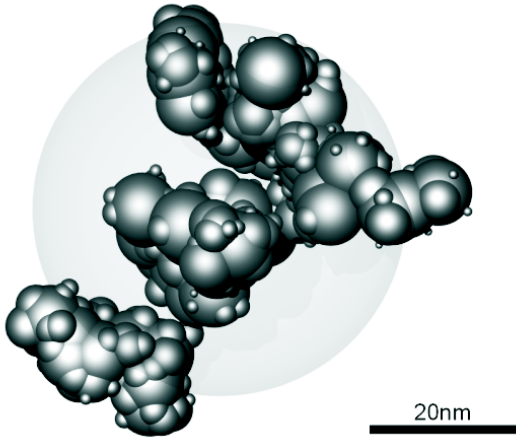

(a) *3D rendering of a particle from flame A1.* $D_c = 49.5\,nm$, $D_f = 2.160$, $D_s = 0.763$.

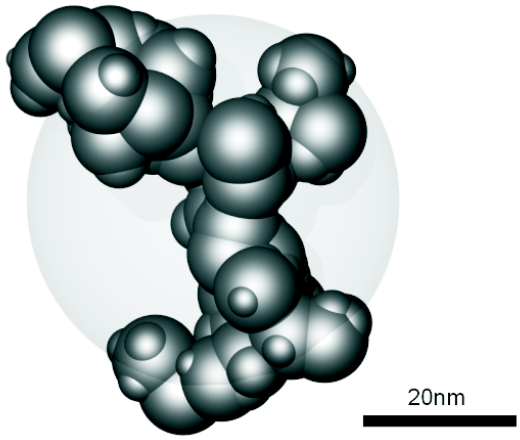

(b) *3D rendering of a particle from flame A3.* $D_c = 50.1\,nm$, $D_f = 2.025$, $D_s = 0.731$.

Figure 5: *Renderings of particles most likely to be found in flames A1 and A3.*

which show that the aggregate from flame A1 is made up of a smaller number of more densely packed and bumpy primary particles than the aggregate from flame A3.

Figures 9 and 10 show the temporal evolution of the joint probability distribution functions of the shape descriptor against the collision diameter for flames A1 and A3. With both flames, the shape of this distribution is set up in the early stages of particle formation and merely expands along the vertical axis of collision diameters. With flame A1, it can be seen that at the end of the flame (Fig. 9(b)) there exists a secondary peak in the bottom left corner where the smallest spherical particles exist, which is not present at the end of flame A3 (Fig. 10(b)).

The particle seen in Fig. 5(a) has a collision diameter of 49.5 nm, a fractal dimension of 2.160 and a shape descriptor of 0.763. This places it in the middle of the contour of maximum value on Fig. 9(b). The particle seen in Fig. 5(b) has a collision diameter of 50.1 nm, a fractal dimension of 2.025 and a shape descriptor of 0.731, placing near the contour of maximum value on Fig. 10(b). The larger particles (Figs. 7 and 8) by contrast lie to the top right of Figs. 9 and 10 respectively.

6 Conclusions

It is usually assumed that inception and evolution of particles in a reactive system, such as soot formation in fossil-fuel flames, can be separated into essentially non-intersecting regimes of particle nucleation, particle coagulation and surface growth, and particle aggregation. Recent studies, using numerical simulations of single-particle trajectories [22, 23] and of "lumped" properties with the method of moments [2], suggested a critical importance of interplay among all these individual

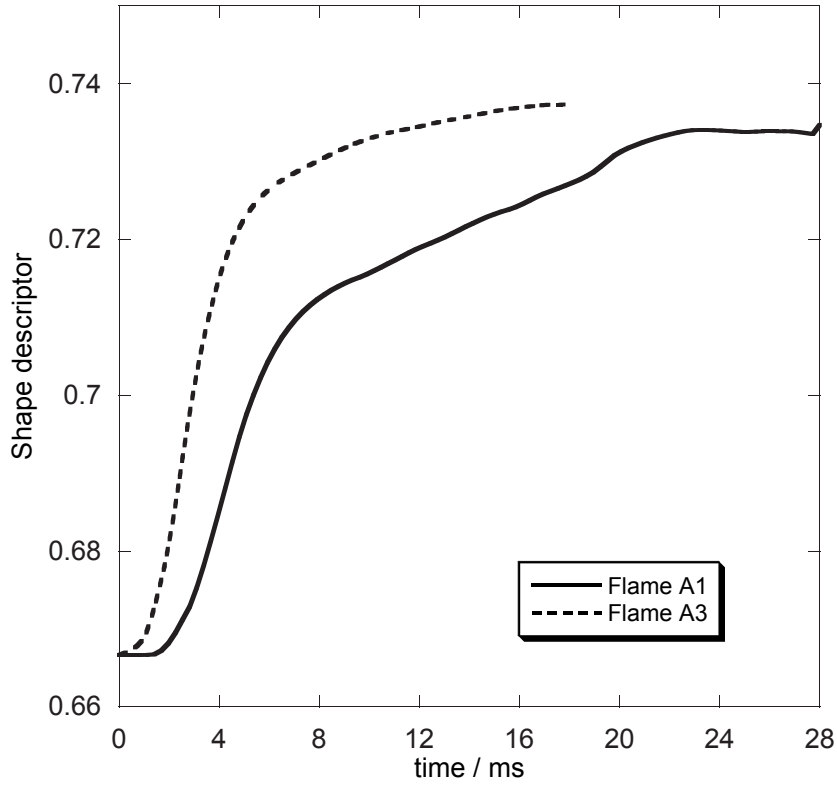

(a) *Temporal evolutions of average D_s in flames A1 and A3*

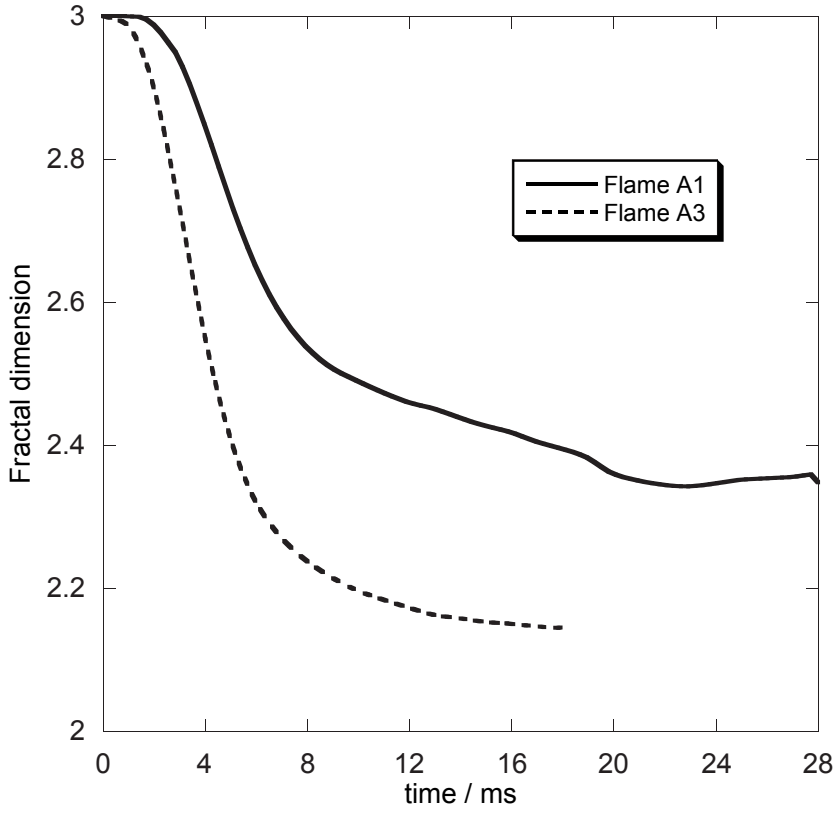

(b) *Temporal evolutions of average D_f in flames A1 and A3*

Figure 6: *Temporal evolution of mean fractal dimension and shape descriptor flames A1 and A3.*

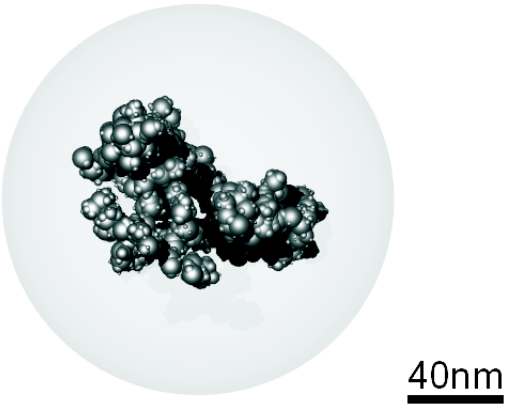

(a) *3D rendering of the largest particle from flame A1.*

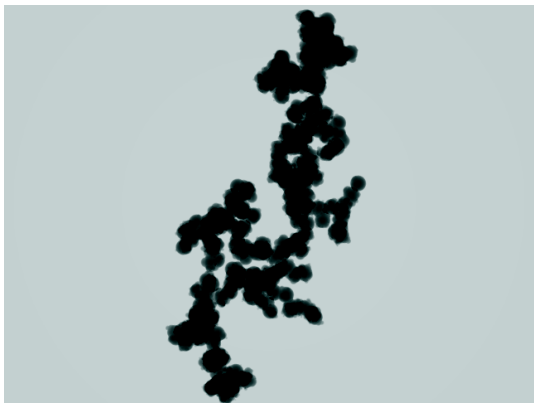

(b) *TEM-style rendering of the largest particle from flame A1.*

Figure 7: *Renderings of largest particle from flame A1.* $D_c = 169\,nm$, $D_f = 1.826$, $D_s = 0.799$.

(a) *3D rendering of the largest particle from flame A3.*

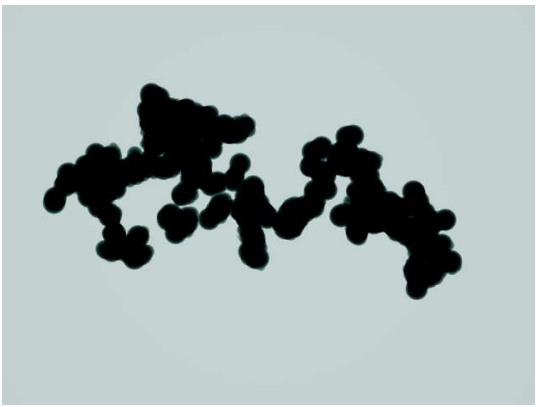

(b) *TEM-style rendering of the largest particle from flame A3.*

Figure 8: *Renderings of largest particle from flame A3.* $D_c = 183\,nm$, $D_f = 1.838$, $D_s = 0.784$.

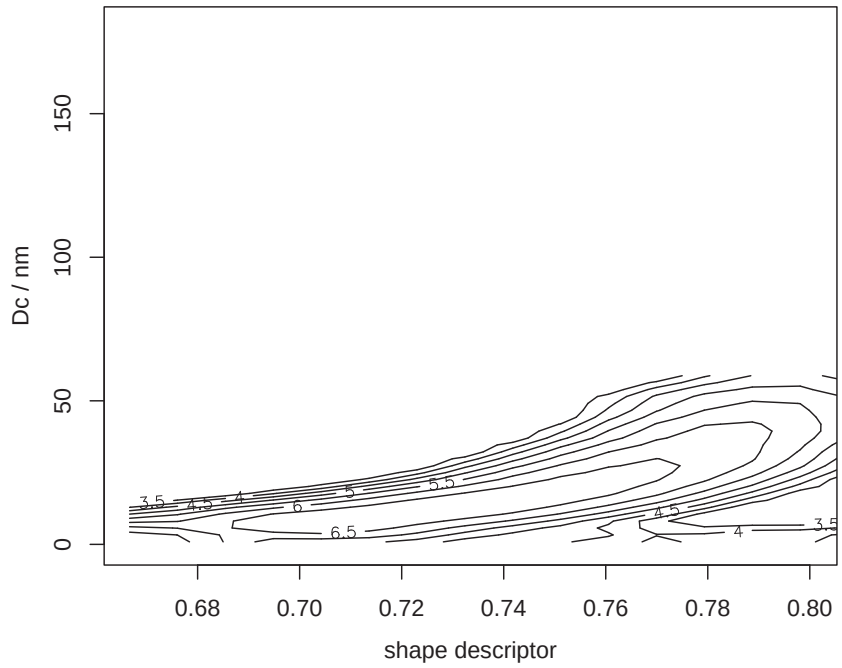

(a) *contour plot @ 7.9 ms*

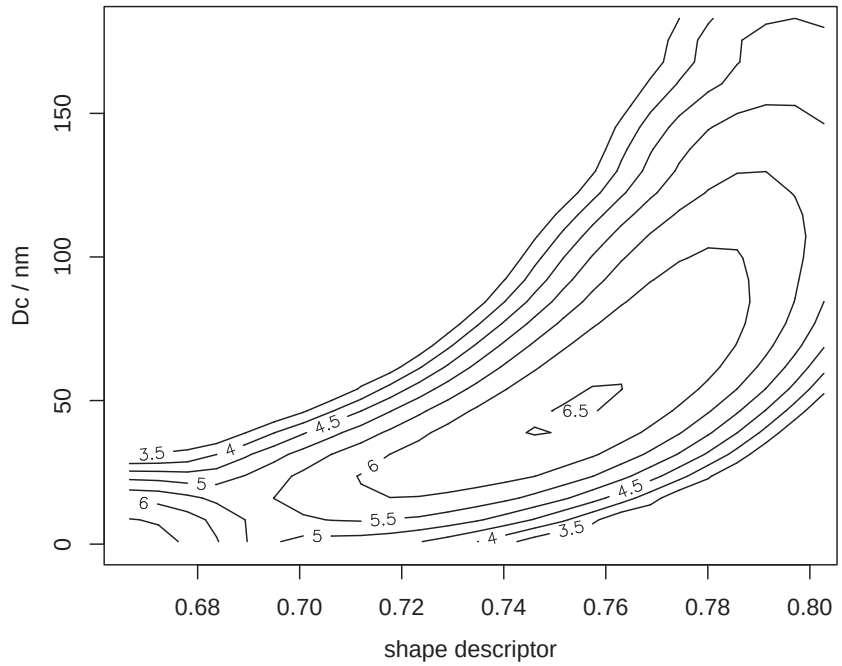

(b) *contour plot @ 28 ms*

Figure 9: *Joint distributions of shape descriptor and collision diameter for flame A1. The numbers on the contours represent the log of the distribution function.*

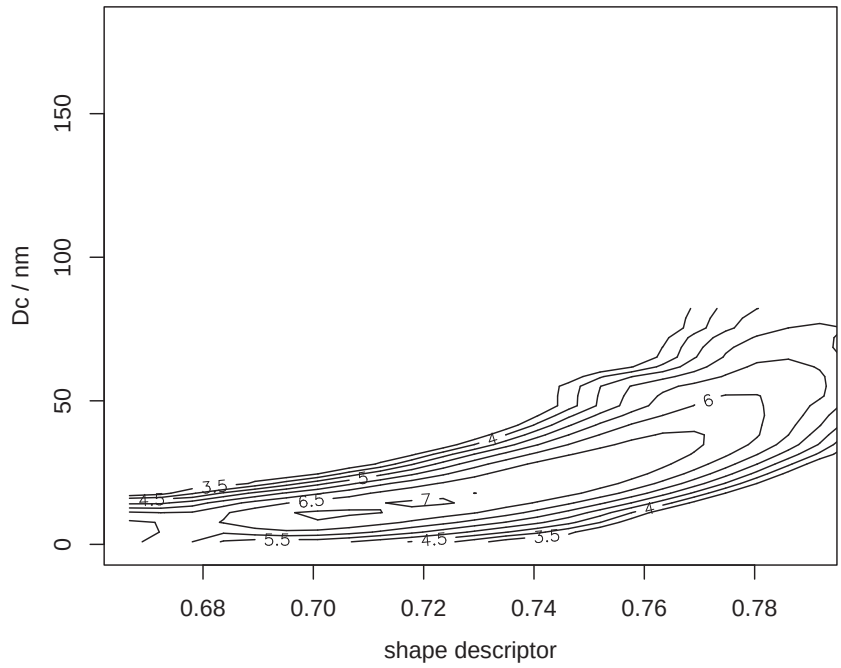

(a) *contour plot @ 5.9 ms*

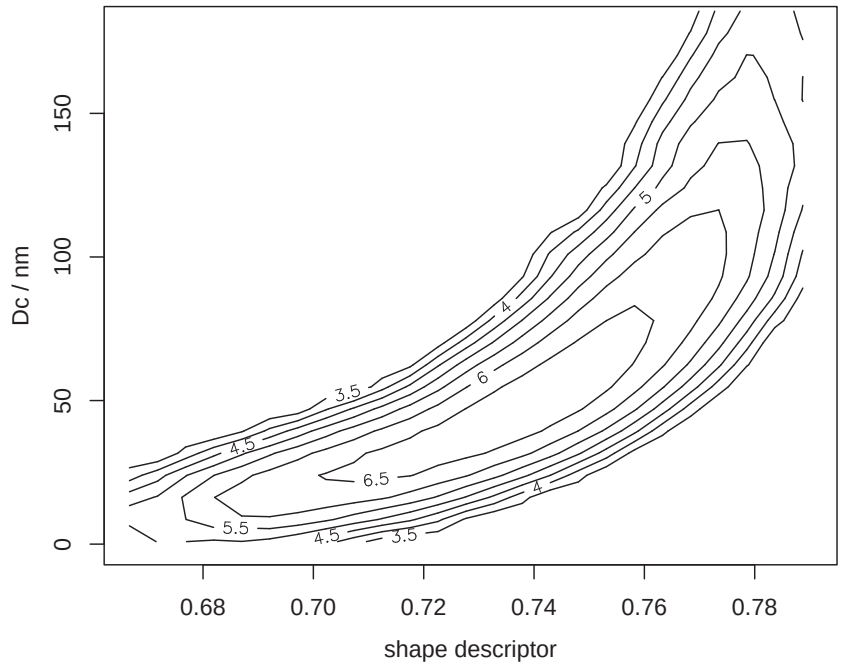

(b) *contour plot @ 18 ms*

Figure 10: *Joint distributions of shape descriptor and collision diameter for flame A3. The numbers on the contours represent the log of the distribution function.*

processes—nucleation, coagulation, and surface growth. Moreover, these results suggested that the transition of spherical, coalescent growth into fractal-like objects is linked directly to the nucleation, as it supplies the abundance of very small primary particles.

The present modelling results, now performed with a numerical model that incorporates all physical processes at a detailed level along with the resolution of individual particles and their distributions, fully supports the earlier suggested mechanistic features. The specific simulations were performed for two flames: with characteristically different bimodal and unimodal soot particle distributions. The present model is able to capture the evolution of soot particle properties observed experimentally in these flames [32]. These results confirm thus that the origin of the differences in the PSDFs is the strength of the nucleation, suggested theoretically two decades ago [8, 4, 17].

Acknowledgments

This work was funded by the EPSRC, grant number GR/R85662/01) for the financial support of Neal Morgan under the title Mathematical and Numerical Analysis of Coagulation-Diffusion Processes in Chemical Engineering. The work at Berkeley was supported by the Director, Office of Energy Research, Office of Basic Energy Sciences, Chemical Sciences, Geosciences and Biosciences Division of the US Department of Energy, under Contract No. DE-AC03-76F00098.

References

[1] J. Appel, H. Bockhorn, and M. Frenklach. Kinetic modeling of soot formation with detailed chemistry and physics: Laminar premixed flames of C_2 hydrocarbons. *Combustion and Flame*, 121:122–136, 2000.

[2] M. Balthasar and M. Frenklach. Detailed kinetic modeling of soot aggregate formation in laminar premixed flames. *Combustion and Flame*, 140:130–145, 2005.

[3] M. Balthasar and M. Kraft. A sochastic approach to calculate the particle size distribution function of soot particles in laminar premixed flames. *Combustion and Flame*, 133:289–298, 2003.

[4] R.A. Dobbins and G.W. Mulholland. Interpretation of optical measurements of flame generated particles. *Combustion Science and Technology*, 40:175–191, 1984.

[5] A. Eibeck and W. Wagner. An efficient stochastic algorithm for studying coagulation dynamics and gelation phenomena. *SIAM Journal of Scientific Computating*, 22(3):802–821, 2000.

[6] M. Frenklach. Method of moments with interpolative closure. *Chemical Engineering Science*, 57:2229–2239, 2002.

[7] M. Frenklach. Reaction mechanism of soot formation in flames. *Phys. Chem. Chem. Phys.*, 2:2028–2037, 2002.

[8] M. Frenklach and S.J. Harris. Aerosol dynamics modeling using the method of moments. *Journal of Colloid and Interface Science*, 118:252–262, 1987.

[9] M. Frenklach and H. Wang. Detailed modeling of soot particle nucleation and growth. *Proceedings of the Combustion Institute*, 23:1559–1566, 1991.

[10] M. Goodson and M. Kraft. An efficient algorithm for simulating nano-particle dynamics. *Journal of Computational Physics*, 183:210–232, 2002.

[11] B.S. Haynes and H.G. Wagner. Soot formation. *Prog. Energy Conmbust. Sci.*, 7:229–167, 1981.

[12] R. Jullien. Transparency effects in cluster-cluster aggregation with linear trajectories. *Journal of Physics A*, 17:L771–L776, 1984.

[13] A. Kazakov and M. Frenklach. *title to go here. Combustion and Flame*, 114:484–510, 1998.

[14] D.B. Kittelson. Engines and nanoparticles: A review. *Journal of Aerosol Science*, 29:575–588, 1997.

[15] Ü.Ö. Köylü, G.M. Faeth, T.L. Farias, and M.G. Carvalho. Fractal and projected structure properties of soot aggregates.

[16] M. Kraft. Modelling of particulate processes. Technical Report 30, c4e Preprint-Series, Cambridge, 2005.

[17] J.D. Landgrebe and S.E. Pratsinis. *title to go here. Ind. Eng. Chem. Res.*, 28:1474–1481, 1989.

[18] D. Lindackers, M.G.D. Strecker, P. Roth, C. Janzen, and S. E. Pratsinis. Formation and growth of sio2 particles in low pressure h2/o2/ar flames doped with sih4. *Combustion Science and Technology*, 123:287–315, 1997.

[19] F. Mauss, Trilken B., H. Breitbach, and N. Peters. *Soot Formation in Combustion - Mechanisms and Models*, page 325. Springer Verlag Berlin, 1994.

[20] C.M. Megaridis and R.A. Dobbins. An integral solution of the aerosol dynamic equation including surface growth reactions. *Combustion Science and Technology*, 63:152–167, 1989.

[21] P. Mitchell. *Monte Carlo Simulations of Soot Aggregation with Simultaneous Surface Growth.* PhD thesis, University of California at Berkeley, 2001.

[22] P. Mitchell and M. Frenklach. Monte carlo simulations of soot aggregation with simultaneous surface growth - why primary particles appear spherical. *Proceedings of the Combustion Institute*, 27:1507–1514, 1998.

[23] P. Mitchell and M. Frenklach. Particle aggregation with simultaneous surface growth. *Phys. Rev. E*, 67:061407, 2003.

[24] Patterson R., J. Singh, M. Balthasar, M. Kraft, and J. Norris. The linear process deferment algorithm: A new technique for solving population balance equations. Technical Report 26, c4e Preprint-Series, Cambridge, 2004.

[25] J. Singh, R. Patterson, M. Balthasar, M. Kraft, and W. Wagner. Modelling soot particle size distribution: Dynamics of pressure regimes. Technical Report 25, c4e Preprint-Series, Cambridge, 2004.

[26] P.T. Spicer, O. Chaoul, S. Tsantilis, and S.E. Pratsinis. Titania formation by ticl4 gas phase oxidation, surface growth and coagulation. *Journal of Aerosol Science*, 33:17–34, 2002.

[27] Z. Sun, R.L. Axelbaum, and B.H. Chao. A multicomponent sectional model applied to flame synthesis of nanoparticles. *Proc. Combust. Inst.*, 29:1063–1069, 2002.

[28] S. Tsantilis and S.E. Pratsinis. Soft- and hard-agglommerate aerosols made at high temperatures. *Langmuir*, 20:5933–5939, 2004.

[29] M. von Smoluchowski. Drei vortrge über diffusion, brownsche molekularbewegung und koagulation von kolloidteilchen. *Phys. Z.*, 17:557–571 and 585–599, 1916.

[30] H. Wang and M. Frenklach. A detailed kinetic modeling study of aromatics formation in laminar premixed acetylene and ethylene flames. *Combustion and Flame*, 110(1-2):173–221, 1997.

[31] Y. Yoshihara, H. Wang, and M. Frenklach. Modeling of nox formation in natural gas fueld diesel combustion. Technical report, Mechanical Engineering, Ritsumeikan University, 1994.

[32] D. Zhao, Z. Yang, Z. Li, M.V. Johnston, and H. H. Wang. Particle size distribution function of incipient soot in laminar premied ethylene flames: Effect of flame temperature. *Proc. Combust. Inst.*, 30:1441–1448, 2005.